Physics Letters A 378 (2014) 2337–2344

Contents lists available at ScienceDirect

Physics Letters A

www.elsevier.com/locate/pla

Tachyonic quantum densities of relativistic electron plasmas: Cherenkov spectra of γ-ray pulsars

Roman Tomaschitz

Department of Physics, Hiroshima University, 1-3-1 Kagami-yama, Higashi-Hiroshima 739-8526, Japan

ARTICLE INFO

Article history:
Received 21 May 2014
Received in revised form 2 June 2014
Accepted 3 June 2014
Available online 6 June 2014
Communicated by V.M. Agranovich

Keywords:
Quantized tachyonic Cherenkov densities
Frequency-dependent tachyon mass
Superluminal radiation in a permeable spacetime
Transversal/longitudinal Cherenkov energy flux
Tachyonic spectral fits to γ-ray pulsars
Subexponential Weibull decay of spectral tails

ABSTRACT

Tachyonic Cherenkov radiation in second quantization can explain the subexponential spectral tails of GeV γ-ray pulsars (Crab pulsar, PSR J1836+5925, PSR J0007+7303, PSR J2021+4026) recently observed with the Fermi-LAT, VERITAS and MAGIC telescopes. The radiation is emitted by a thermal ultra-relativistic electron plasma. The Cherenkov effect is derived from a Maxwell–Proca field with negative mass-square in a dispersive spacetime. The frequency variation of the tachyon mass results in $\exp(-\hat{\beta}\omega^{1-\rho})$ attenuation of the asymptotic Cherenkov energy flux, where $\hat{\beta}$ is a decay constant related to the electron temperature and ρ is the frequency scaling exponent of the tachyon mass. An exponent in the range $0 < \rho < 1$ can reproduce the observed subexponential decay of the energy flux. For the Crab pulsar, we find $\rho = 0.81 \pm 0.02$, inferred from the substantially weaker-than-exponential decay of its spectral tail measured by MAGIC over an extended energy range. The scaling exponent ρ determines whether the group velocity of the tachyonic γ-rays is sub- or superluminal.

1. Introduction

Stunning high-precision spectra of several γ-ray pulsars which defy traditional radiation models have recently been recorded by the Fermi satellite and the terrestrial γ-ray telescopes MAGIC and VERITAS. An account of these developments can be found in the review [1]. These spectra are difficult to explain, as the spectral tails decay more slowly than an exponential cutoff but faster than a power law, so that something in between these two extremes is needed.

Here, we will show that a Weibull [2] decay factor $\exp(-(E/E_0)^\delta)$, $0 < \delta < 1$, in the asymptotic energy flux can reproduce the very accurately measured subexponential decay of the spectral tails. To this end, we will perform spectral fits to four Fermi-LAT pulsars (including the Crab pulsar), covering a representative range of shape parameters δ. First, however, we have to find a radiation model which produces an energy flux admitting asymptotic Weibull decay; this is the principal aim of this article. Time-honored electromagnetic radiation mechanisms such as inverse-Compton scattering or synchrotron and curvature radiation result in straight exponential cutoffs ($\delta = 1$) if the cross-section or radiation density is averaged over a relativistic equilibrated or non-thermal electronic source plasma.

We will invoke the tachyonic Cherenkov effect based on a Maxwell–Proca field theory with negative mass-square, and demonstrate that the Cherenkov flux density produced by an ultra-relativistic electron population decays subexponentially. This holds true in the quasiclassical regime as well as in the extreme quantum limit of the Cherenkov flux, with different shape parameters δ in the Weibull exponential. The spectral fits to the GeV pulsar spectra will be performed in the semiclassical regime, but the quantum limit is inescapable at sufficiently high frequency and can be manifested in TeV γ-rays.

Apart from subexponential Weibull decay, which is the main focus, there are also other features of tachyonic Cherenkov radiation quite different from electromagnetic radiation. For instance, three degrees of polarization, two transversal and one longitudinal due to the tachyonic mass-square of the radiation field. The Cherenkov emission angles differ for transversal and longitudinal γ-rays. Most importantly, the γ-rays can have a slightly superluminal group velocity depending on the Weibull shape parameter δ, and we will illustrate this with a pulsar spectrum.

In Section 2, we introduce the Lagrangian of the underlying field theory, a Proca field with negative mass-square, coupled to dispersive permeability tensors and an external spinor current. We discuss tachyonic radiation densities in second quantization, their

E-mail address: tom@geminga.org.

http://dx.doi.org/10.1016/j.physleta.2014.06.005
0375-9601/

polarization components and the effect of electron spin. We determine the frequency intervals in which Cherenkov radiation from an inertial Dirac electron current is possible, depending on the permeabilities in the Lagrangian and the electronic Lorentz factor, and derive the Cherenkov emission angles. The quantized electromagnetic Cherenkov densities [3–7] are recovered in the limit of zero tachyon mass, and the classical tachyonic radiation densities [8,9] for small tachyon–electron mass ratio.

To relate the tachyonic Cherenkov densities to pulsar spectra, we have to average them over a relativistic electron plasma, cf. Section 3. We consider thermal equilibrium distributions as well as non-thermal power-law distributions for the radiating electron populations of the pulsars. The averaged differential flux densities are then fitted to the measured GeV pulsar spectra. There is a longitudinal radiation component, which is even more intense than the linearly polarized transversal radiation in the semiclassical regime. A second transversal degree of polarization emerges in the quantum regime, where the longitudinal energy flux weakens.

In Section 4, we study tachyonic flux densities in the quasiclassical regime. We explain the frequency variation of the tachyon mass and the tachyonic fine-structure constant, specializing to permeability tensors which give identical dispersion relations and group velocities for transversal and longitudinal quanta. Whether the group velocity is sub- or superluminal depends on the frequency variation of the tachyon mass, which is inferred from the decaying spectral tails of the pulsars.

In Section 5, we test the averaged tachyonic Cherenkov densities by performing spectral fits to the γ-ray pulsars PSR J1836+5925, PSR J0007+7303, PSR J2021+4026 and the Crab pulsar [10,11]. In this way, the scaling exponent ρ of the frequency-dependent tachyon mass $\propto\omega^\rho$ can be inferred. The decay of the spectral tails is weaker than exponential because of the Weibull decay factor $\exp(-\hat\beta\omega^{1-\rho})$, $0<\rho<1$, in the asymptotic flux density, the decay exponent $\hat\beta$ being related to the temperature of the ultra-relativistic electron plasma and the tachyonic mass amplitude. (The above mentioned Weibull slope is thus $\delta=1-\rho$.) For $\rho<1/2$, the radiation is superluminal [12,13], as happens for pulsar PSR J1836+5925. In the case of the Crab pulsar, the tachyon mass admits a scaling exponent ρ close to one, so that the Weibull exponential approximates power-law decay of the spectral tail, and the radiation is slightly subluminal despite of the tachyonic mass-square in the dispersion relations, cf. Section 6. Apart from the tachyonic Cherenkov effect discussed here, the thermodynamics of superluminal signal transfer has been studied in Ref. [14], electromagnetic radiation by acceleration of superluminal charges in Ref. [15], and Cherenkov radiation from superluminally rotating light spots in Ref. [16].

2. Quantized tachyonic Cherenkov densities of relativistic electrons

The Cherenkov radiation densities stated below are derived from the Lagrangian [9]

$$\hat L=-\frac14\hat F_{\mu\nu}g_F^{\mu\alpha}g_F^{\nu\beta}\hat F^*_{\alpha\beta}+\frac12 m_{\rm t}^2\hat A_\mu g_A^{\mu\nu}\hat A^*_\nu +\frac12\big(\hat A_\mu g_J^{\mu\nu}\hat j^*_\nu+\hat A^*_\mu g_J^{\mu\nu}\hat j_\nu\big), \tag{2.1}$$

where $\hat F_{\mu\nu}(\mathbf{x},\omega)$ is the Fourier transform $\int_{-\infty}^{\infty}F_{\mu\nu}(\mathbf{x},t)\mathrm{e}^{\mathrm{i}\omega t}\mathrm{d}t$ of the field tensor $F_{\mu\nu}=A_{\nu,\mu}-A_{\mu,\nu}$ and $\hat A_\mu$ and $\hat j_\nu(\mathbf{x},\omega)$ are the transforms of the 4-potential and external current. The tachyonic radiation field is modeled after electrodynamics, a Proca field with negative mass-square, minimally coupled to an electron current in a dispersive spacetime, the Minkowski metric being replaced by permeability tensors $g^{\mu\nu}_{F,A,J}(\omega)$. $m_{\rm t}^2(\omega)$ is the frequency-dependent tachyonic mass-square. ($m_{\rm t}^2>0$ with the sign conventions in (2.1).) The first term in (2.1) containing $g_F^{\mu\nu}$ is analogous to the electrodynamic Lagrangian in a dielectric medium, in manifestly covariant notation. A second permeability tensor $g_A^{\mu\nu}$ enters in the mass term, generating different dispersion relations and group velocities for transversal and longitudinal modes. The isotropic tensors $g^{\mu\nu}_{A,F}$ are defined by positive dimensionless permeabilities $\varepsilon(\omega)$, $\mu(\omega)$, $\mu_0(\omega)$ and $\varepsilon_0(\omega)$,

$$g_A^{00}=-\varepsilon_0,\qquad g_A^{ij}=\frac{\delta^{ij}}{\mu_0},\qquad g_F^{00}=-\mu^{1/2}\varepsilon,\qquad g_F^{ij}=\frac{\delta^{ij}}{\mu^{1/2}}, \tag{2.2}$$

with $g_A^{0i}=g_F^{0i}=0$. In vacuum, $\varepsilon=\varepsilon_0=1$ and $\mu=\mu_0=1$ (Heaviside–Lorentz system). Greek indices are raised and lowered with the Minkowski metric $\eta_{\mu\nu}=\mathrm{diag}(-1,1,1,1)$. The 3D field strengths are $\hat E_k=\hat F_{k0}$ and $\hat B^k=\varepsilon^{kij}\hat F_{ij}/2$. ($\varepsilon^{kij}$ is the Levi-Civita tensor.) The inductive 4-potential reads $\hat C^\mu=g_A^{\mu\nu}\hat A_\nu$ and the inductive field tensor $\hat H^{\mu\nu}=g_F^{\mu\alpha}g_F^{\nu\beta}\hat F_{\alpha\beta}$. The 3D inductions are $\hat D^l=\hat H^{0l}$, $\hat H_i=\varepsilon_{ikl}\hat H^{kl}/2$, so that the constitutive relations read $\hat{\mathbf D}=\varepsilon\hat{\mathbf E}$, $\hat{\mathbf B}=\mu\hat{\mathbf H}$ and $\hat{\mathbf A}=\mu_0\hat{\mathbf C}$, $\hat C_0=\varepsilon_0\hat A_0$. The permeability tensor $g_J^{\mu\nu}$ in Lagrangian (2.1) couples the external current to the field,

$$g_J^{00}=-\Omega_0(\omega),\qquad g_J^{mn}=\frac{\delta^{mn}}{\Omega(\omega)},\qquad g_J^{k0}=0. \tag{2.3}$$

The 'dressed' current $\hat j^\mu_\Omega=g_J^{\mu\nu}\hat j_\nu$ in the Lagrangian amounts to a varying coupling constant if $\Omega_0(\omega)$ coincides with $1/\Omega(\omega)$ [8], so that $\hat j^\mu_\Omega=\hat j^\mu/\Omega$, which is assumed from now on.

The external current $\hat j^\mu$ is generated by a uniformly moving subluminal charge q with mass m and Lorentz factor γ. When quantizing, we use an inertial Dirac current. The Cherenkov emission of the charge has two transversal and one longitudinal polarization components. The spectral densities in second quantization read, for the two linear transversal polarizations,

$$p^{\mathrm{T}(1)}_{\rm spin}(\omega)=\frac{q^2}{4\pi}\frac{\mu(\omega)}{\Omega^2(\omega)}\frac{M_{\rm T}^2\omega}{\omega^2+M_{\rm T}^2}\bigg(1+\frac{\omega^2}{M_{\rm T}^2}\bigg)\frac{M_{\rm T}^2}{4m^2}\frac{\Theta(D_{\rm t}^{\rm T})}{\gamma\sqrt{\gamma^2-1}}, \tag{2.4}$$

$$p^{\mathrm{T}(2)}_{\rm spin}(\omega)=\frac{q^2}{4\pi}\frac{\mu(\omega)}{\Omega^2(\omega)}\frac{M_{\rm T}^2\omega}{\omega^2+M_{\rm T}^2}\bigg[\gamma^2-\frac{\omega}{m}\gamma-\frac{M_{\rm T}^2}{4m^2} -\bigg(1+\frac{\omega^2}{M_{\rm T}^2}\bigg)\bigg(1-\frac{M_{\rm T}^2}{4m^2}\bigg)\bigg]\frac{\Theta(D_{\rm t}^{\rm T})}{\gamma\sqrt{\gamma^2-1}}, \tag{2.5}$$

so that $p^{\rm T}_{\rm spin}=p^{\mathrm{T}(1)}_{\rm spin}+p^{\mathrm{T}(2)}_{\rm spin}$ is the total transversal density. The various symbols in (2.4) and (2.5) are defined below. The longitudinal radiation component is

$$p^{\rm L}_{\rm spin}(\omega)=\frac{q^2}{4\pi}\frac{m_{\rm t}^2(\omega)\varepsilon_0(\omega)}{\Omega^2(\omega)\varepsilon^2(\omega)}\frac{\omega}{\omega^2+M_{\rm L}^2}\bigg(\gamma^2-\frac{\omega}{m}\gamma-\frac{M_{\rm L}^2}{4m^2}\bigg)\frac{\Theta(D_{\rm t}^{\rm L})}{\gamma\sqrt{\gamma^2-1}}, \tag{2.6}$$

where m denotes the electron mass, γ the electronic Lorentz factor and $m_{\rm t}(\omega)>0$ the frequency-dependent tachyon mass. The permeabilities ε, μ, μ_0 and ε_0 are positive. The dimensionless constant $\alpha_{\rm t0}=q^2/(4\pi\hbar c)$ is the tachyonic counterpart to the electric fine-structure constant $e^2/(4\pi\hbar c)\approx1/137$. $\Omega^2(\omega)$ is the scale factor of the frequency-dependent tachyonic fine-structure constant $\alpha_{\rm t}(\omega)=\alpha_{\rm t0}/\Omega^2(\omega)$, see after (2.3). We introduce the rescaled tachyon mass

$$\hat{m}_{\rm t}(\omega)=\frac{m_{\rm t}(\omega)}{\sqrt{\varepsilon(\omega)\mu_0(\omega)}}, \tag{2.7}$$

and write the generalized transversal and longitudinal mass-squares $M^2_{\rm T,L}$ in densities (2.4)–(2.6) as

$$M^2_{\rm T}=(\varepsilon\mu-1)\omega^2+\hat{m}^2_{\rm t}\varepsilon\mu,\qquad M^2_{\rm L}=(\varepsilon_0\mu_0-1)\omega^2+\hat{m}^2_{\rm t}\varepsilon_0\mu_0. \tag{2.8}$$

These mass-squares must be positive for radiation to occur, see after (2.14). Finally, the factor $\Theta(D^{\rm T,L}_{\rm t})$ in the spectral densities (2.4)–(2.6) is the Heaviside step function with argument

$$D^{\rm T,L}_{\rm t}(\omega,\gamma)=k_{\rm T,L}(\omega)\frac{\sqrt{\gamma^2-1}}{\gamma}-\omega+\frac{\omega^2-k^2_{\rm T,L}(\omega)}{2m\gamma}, \tag{2.9}$$

where $k_{\rm T,L}(\omega)$ are the transversal/longitudinal wavenumbers defined by the dispersion relations

$$k^2_{\rm T}(\omega)=\varepsilon\mu\omega^2+m^2_{\rm t}\frac{\mu}{\mu_0},\qquad k^2_{\rm L}(\omega)=\varepsilon_0\mu_0\omega^2+m^2_{\rm t}\frac{\varepsilon_0}{\varepsilon}, \tag{2.10}$$

so that $k^2_{\rm T,L}=\omega^2+M^2_{\rm T,L}$. The wavenumbers (2.10) are identical only if the permeabilities satisfy $\varepsilon_0\mu_0=\varepsilon\mu$. To derive the radiation densities (2.4)–(2.6), it suffices to calculate the asymptotic transversal and longitudinal radiation fields in dipole approximation (see Eq. (3.1) of Ref. [8]) and to use the integral representation of the asymptotic flux vectors stated in Eq. (3.7) of Ref. [8], replacing the classical transversal/longitudinal current components in this integral representation by the respective matrix elements of the spinor current of the radiating inertial charge q as explained in Refs. [17–20] for the vacuum case. The polarized power components are $P^{{\rm T}(j),{\rm L}}=\int_0^{m\gamma}p^{{\rm T}(j),{\rm L}}_{\rm spin}(\omega){\rm d}\omega$, where the upper integration boundary is the energy $m\gamma$ of the radiating charge. The total transversal power is $P^{\rm T}=P^{{\rm T}(1)}+P^{{\rm T}(2)}$, and the total power radiated is $P=P^{\rm T}+P^{\rm L}$. If we use a spinless Klein–Gordon current as radiation source instead of the electronic Dirac current, the quantized radiation densities read $p^{{\rm T}(1)}_{\rm KG}(\omega)=0$ and

$$p^{{\rm T}(2)}_{\rm KG}(\omega)=\frac{q^2}{4\pi}\frac{\mu(\omega)}{\Omega^2(\omega)}\frac{M^2_{\rm T}\omega}{\omega^2+M^2_{\rm T}}\left[\gamma^2-\frac{\omega}{m}\gamma-\frac{M^2_{\rm T}}{4m^2}-\left(1+\frac{\omega^2}{M^2_{\rm T}}\right)\right]\frac{\Theta(D^{\rm T}_{\rm t})}{\gamma\sqrt{\gamma^2-1}}, \tag{2.11}$$

$$p^{\rm L}_{\rm KG}(\omega)=\frac{q^2}{4\pi}\frac{m^2_{\rm t}(\omega)\varepsilon_0(\omega)}{\Omega^2(\omega)\varepsilon^2(\omega)}\frac{\omega}{\omega^2+M^2_{\rm L}}\left(\gamma^2-\frac{\omega}{m}\gamma+\frac{1}{4}\frac{\omega^2}{m^2}\right)\frac{\Theta(D^{\rm L}_{\rm t})}{\gamma\sqrt{\gamma^2-1}}. \tag{2.12}$$

Here, we use the same notation as in (2.4)–(2.6). The transversal component $p^{{\rm T}(1)}_{\rm spin}$ in (2.4) is thus exclusively due to the electron spin. The vacuum version of densities (2.11) and (2.12) has been derived in Ref. [18].

The zeros of the argument $D^{\rm T,L}_{\rm t}(\omega,\gamma)$ in the Heaviside function, cf. (2.9), determine the frequency intervals (at fixed γ) in which $D^{\rm T,L}_{\rm t}(\omega,\gamma)>0$, i.e. the transversal and longitudinal spectrum radiated by an inertial spinning or spinless charge of mass m with Lorentz factor $\gamma>1$. Alternatively, we may keep ω fixed, so that the zeros of $D^{\rm T,L}_{\rm t}(\omega,\gamma)$ with respect to the second variable determine the γ intervals $D^{\rm T,L}_{\rm t}(\omega,\gamma)>0$ in which a frequency ω can be radiated. That is, the charge must have a Lorentz factor in these intervals to radiate at a given frequency ω. In addition, the energy condition $m\gamma\geq\omega$ has to be satisfied. We substitute the dispersion relations (2.10) into $D^{\rm T,L}_{\rm t}(\omega,\gamma)$ so that inequality $D^{\rm T,L}_{\rm t}(\omega,\gamma)\geq 0$ is equivalent to

$$\Delta^{\rm T,L}_{\rm t}(\omega,\gamma)=M^2_{\rm T,L}\left[\gamma^2-\frac{\omega}{m}\gamma-\left(\frac{M^2_{\rm T,L}}{4m^2}+\frac{\omega^2}{M^2_{\rm T,L}}+1\right)\right]\geq 0. \tag{2.13}$$

If $M^2_{\rm T,L}(\omega)>0$, the second-order polynomial $\Delta^{\rm T,L}_{\rm t}(\omega,\gamma)$ has a root $\gamma=\gamma^{\rm T,L}_{\rm min}$ satisfying $\gamma^{\rm T,L}_{\rm min}\geq 1$ as well as $m\gamma^{\rm T,L}_{\rm min}\geq\omega$, which is given by

$$\gamma^{\rm T,L}_{\rm min}(\omega)=\frac{\omega}{M_{\rm T,L}}\frac{M_{\rm T,L}}{2m}+\sqrt{\left(1+\frac{M^2_{\rm T,L}}{4m^2}\right)\left(1+\frac{\omega^2}{M^2_{\rm T,L}}\right)}. \tag{2.14}$$

Inequality $\Delta^{\rm T,L}_{\rm t}(\omega,\gamma)\geq 0$ in (2.13) is then equivalent to $\gamma\geq\gamma^{\rm T,L}_{\rm min}(\omega)$.

Inequality (2.13) cannot be satisfied for any $\gamma\geq 1$ if $M^2_{\rm T,L}$ is negative. [Inequality (2.13) is not satisfied for $\gamma\to\infty$ if $M^2_{\rm T,L}<0$. Thus it can only hold for γ below $\gamma^{\rm T,L}_{\rm min}(\omega)$. Inequality $\gamma^{\rm T,L}_{\rm min}(\omega,M^2_{\rm T,L})>1$ is equivalent to $M^4_{\rm T,L}+4m\omega M^2_{\rm T,L}+4m^2\omega^2<0$ if $M^2_{\rm T,L}<0$. This polynomial has a double-root $M^2_{\rm T,L}=-2m\omega$, so that the inequality cannot be satisfied. Accordingly, $\gamma^{\rm T,L}_{\rm min}(\omega)<1$ if $M^2_{\rm T,L}<0$.] Thus we only need to consider frequency intervals in which the mass-squares $M^2_{\rm T,L}(\omega)$ are positive, as Cherenkov radiation cannot occur for negative $M^2_{\rm T,L}$. If $M^2_{\rm T}(\omega)$ is positive and $M^2_{\rm L}(\omega)$ negative, only transversal emission occurs at this frequency, and vice versa.

By expanding Eq. (2.14) in the parameter $M_{\rm T,L}/(2m)\ll 1$ in leading order, we find the limit $\gamma^{\rm T,L}_{\rm min}(\omega)\sim\sqrt{1+\omega^2/M^2_{\rm T,L}}$ obtained in Ref. [8] for classical Cherenkov radiation. The mass m of the subluminal radiating charge does not enter in the classical Cherenkov densities. In fact, the classical densities [8] can be recovered by performing the limit $m\to\infty$ in the quantum densities (2.4)–(2.6). The quantized electromagnetic Cherenkov densities [7] are recovered in the limit of vanishing tachyon mass, $m_{\rm t}(\omega)\to 0$, if we replace the tachyonic fine-structure constant $q^2/(4\pi\Omega^2)$ by the electric counterpart $e^2/(4\pi)$, cf. after (2.6). In this electromagnetic limit, the permeabilities have to satisfy $\varepsilon\mu>1$, otherwise the generalized mass-square $M^2_{\rm T}$ is not positive, cf. (2.8), whereas tachyonic Cherenkov radiation is quite possible for $0<\varepsilon\mu\leq 1$ and $0<\varepsilon_0\mu_0\leq 1$.

Applying energy–momentum conservation, we find the Cherenkov emission angle $\theta_{\rm T,L}$ of transversal/longitudinal tachyonic quanta as

$$\cos\theta_{\rm T,L}=\frac{2E\omega+M^2_{\rm T,L}}{2\sqrt{\omega^2+M^2_{\rm T,L}}\sqrt{E^2-m^2}}, \tag{2.15}$$

with electron energy $E=m\gamma$ and mass-square $M^2_{\rm T,L}$ in (2.8). $\theta_{\rm T,L}$ is the angle between the tachyonic wave vector and the velocity of the radiating charge. Since $E\geq\omega$, $\cos\theta_{\rm T,L}$ is positive, so that $\theta_{\rm T,L}$ varies in the interval $0\leq\theta_{\rm T,L}<\pi/2$, and the radiation is thus emitted into a forward cone. This holds true for positive permeabilities; emission into a backward cone can occur in the case of a negative refractive index [21]. We also note that inequality $\cos\theta_{\rm T,L}\leq 1$ is equivalent to $2ED^{\rm T,L}_{\rm t}(\omega,\gamma)\geq 0$, cf. (2.9). For $E\to m$, the right-hand side of Eq. (2.15) diverges; the minimal electron energy $E^{\rm T,L}_{\rm min}$ for emission is thus obtained by solving $\cos\theta_{\rm T,L}=1$, and we find $E^{\rm T,L}_{\rm min}=m\gamma^{\rm T,L}_{\rm min}(\omega)$, cf. (2.14). The energy conditions $E^{\rm T,L}_{\rm min}\geq m$ and $E^{\rm T,L}_{\rm min}\geq\omega$ hold, and $\theta_{\rm T,L}(E^{\rm T,L}_{\rm min})=0$. In the opposite limit, $E\to\infty$, we find the maximal emission angle

$$\cos\theta_{\rm T,L}(E\to\infty)=\cos\theta^{\rm T,L}_{\rm max}=\frac{\omega}{\sqrt{\omega^2+M^2_{\rm T,L}}}, \tag{2.16}$$

so that $0 \le \theta_{\mathrm{T,L}} \le \theta_{\max}^{\mathrm{T,L}} < \pi/2$. Finally, the emission angle for classical tachyonic Cherenkov radiation is recovered in the limit $m \to \infty$, $\cos\theta_{\mathrm{T,L}}^{\mathrm{cl}} = \omega/(k_{\mathrm{T,L}}\upsilon)$, where $\upsilon = \sqrt{1-1/\gamma^2}$ is the velocity of the radiating subluminal charge and $k_{\mathrm{T,L}}$ are the tachyonic wavenumbers (2.10).

3. Polarized tachyonic flux densities of an ultra-relativistic electron plasma

We average the tachyonic Cherenkov densities (2.4)–(2.6) over an electronic power-law distribution [22–25],

$$\mathrm{d}\rho_{\alpha,\beta}(\gamma) = A_{\alpha,\beta}\gamma^{-\alpha-1}\mathrm{e}^{-\beta\gamma}\sqrt{\gamma^2-1}\mathrm{d}\gamma, \tag{3.1}$$

parametrized with the electronic Lorentz factor γ. $A_{\alpha,\beta}$ is a dimensionless normalization constant, $\beta = m/(k_{\mathrm{B}}T)$ is the dimensionless temperature parameter and m the electron mass. A Maxwell–Boltzmann equilibrium distribution requires the electron index $\alpha = -2$. The spectral average of the radiation densities is carried out as

$$\begin{aligned}\big\langle p^{\mathrm{T}(j),\mathrm{L}}(\omega)\big\rangle_{\alpha,\beta} &= B^{\mathrm{T}(j),\mathrm{L}}\big(\omega,\gamma_{\min}^{\mathrm{T,L}}(\omega)\big),\\ B^{\mathrm{T}(j),\mathrm{L}}(\omega,\gamma) &= \int_{\gamma}^{\infty} p_{\mathrm{spin}}^{\mathrm{T}(j),\mathrm{L}}(\omega,\gamma)\mathrm{d}\rho_{\alpha,\beta}(\gamma),\end{aligned} \tag{3.2}$$

where $\gamma_{\min}^{\mathrm{T,L}}$ is the minimal Lorentz factor in (2.14). We will write $B^{\mathrm{T}(j),\mathrm{L}}$ for $B^{\mathrm{T}(j),\mathrm{L}}(\omega,\gamma_{\min}^{\mathrm{T,L}}(\omega))$. The unpolarized radiation density is $\langle p^{\mathrm{T+L}}(\omega)\rangle_{\alpha,\beta} = B^{\mathrm{T+L}}$, with $B^{\mathrm{T+L}} = B^{\mathrm{T}} + B^{\mathrm{L}}$ and $B^{\mathrm{T}} = B^{\mathrm{T}(1)} + B^{\mathrm{T}(2)}$. The differential energy flux $F_\omega^{\mathrm{T}(j),\mathrm{L}}$ and the differential number flux $\mathrm{d}N^{\mathrm{T}(j),\mathrm{L}}/\mathrm{d}\omega$ are related to the spectral functions $B^{\mathrm{T}(j),\mathrm{L}}(\omega,\gamma_{\min}^{\mathrm{T,L}}(\omega))$ by

$$\omega^k F_\omega^{\mathrm{T}(j),\mathrm{L}} = \omega^{1+k}\frac{\mathrm{d}N^{\mathrm{T}(j),\mathrm{L}}}{\mathrm{d}\omega} = \frac{\omega^k B^{\mathrm{T}(j),\mathrm{L}}}{4\pi d^2}, \tag{3.3}$$

where d is the distance to the source. It is customary in high-frequency bands to write E for the energy ω of the γ-rays ($\hbar = c = 1$), if no confusion with the electron energy $E = m\gamma$ can arise. We have rescaled $F_\omega^{\mathrm{T}(j),\mathrm{L}}$ with a power ω^k to make steep spectral slopes better visible, using $k = 1$ in the spectral fits. The total differential flux $\omega^k F_\omega^{\mathrm{T+L}}$ [$(\mathrm{GeV})^k\,\mathrm{cm}^{-2}\,\mathrm{s}^{-1}$] is obtained by adding the polarization components, substituting $B^{\mathrm{T+L}}$ into (3.3).

To make the flux densities (3.3) more explicit, we start by defining the combined amplitude and the rescaled frequency and mass parameters

$$a_{\mathrm{t}} = \frac{\alpha_{\mathrm{t}0}A_{\alpha,\beta}}{4\pi d^2}\beta^{\alpha-1}, \qquad \hat\omega_{\mathrm{T,L}} = \frac{\omega}{M_{\mathrm{T,L}}}, \qquad \hat M_{\mathrm{T,L}} = \frac{M_{\mathrm{T,L}}}{2m}, \tag{3.4}$$

with $M_{\mathrm{T,L}}(\omega)$ in (2.8). The constants $A_{\alpha,\beta}$, β and α denote normalization factor, temperature parameter and electron index of the source distribution (3.1). $\alpha_{\mathrm{t}0} = q^2/(4\pi)$, cf. after (2.6), d is the source distance, cf. (3.3), and m the electron mass. The minimal electronic Lorentz factor (2.14) can now be written as

$$\gamma_{\min}^{\mathrm{T,L}}(\omega) = \hat\omega_{\mathrm{T,L}}\hat M_{\mathrm{T,L}} + \sqrt{1+\hat M_{\mathrm{T,L}}^2}\sqrt{1+\hat\omega_{\mathrm{T,L}}^2}. \tag{3.5}$$

The quasiclassical regime is attained for $\hat M_{\mathrm{T,L}}(\omega) \ll 1$, the classical limit being $\hat M_{\mathrm{T,L}} = 0$ (that is $m \to \infty$, so that the electron mass drops out in the radiation densities), and the quantum regime is realized in the opposite limit, $\hat M_{\mathrm{T,L}} \gg 1$, cf. Section 6.

The spectral average (3.2) can be expressed in terms of incomplete gamma functions. The averaged transversal polarization components (2.4) and (2.5) read

$$\begin{aligned}\omega^k F_\omega^{\mathrm{T}(1)} &= \frac{a_{\mathrm{t}}\mu(\omega)}{\Omega^2(\omega)}\frac{1}{(\beta\gamma)^{\alpha+2}}\frac{\omega^{1+k}}{\hat\omega_{\mathrm{T}}^2+1}\\ &\quad\times\beta^2\big(1+\hat\omega_{\mathrm{T}}^2\big)\hat M_{\mathrm{T}}^2(\beta\gamma)^{\alpha+2}\Gamma(-\alpha-1,\beta\gamma)\end{aligned} \tag{3.6}$$

and

$$\begin{aligned}\omega^k F_\omega^{\mathrm{T}(2)} &= \frac{a_{\mathrm{t}}\mu(\omega)}{\Omega^2(\omega)}\frac{1}{(\beta\gamma)^{\alpha+2}}\frac{\omega^{1+k}}{\hat\omega_{\mathrm{T}}^2+1}\\ &\quad\times\big\{\big[\alpha(\alpha+1)+2(\alpha+1)\beta\hat\omega_{\mathrm{T}}\hat M_{\mathrm{T}}-\beta^2\hat M_{\mathrm{T}}^2\\ &\quad-\beta^2\big(1+\hat\omega_{\mathrm{T}}^2\big)\big(1-\hat M_{\mathrm{T}}^2\big)\big](\beta\gamma)^{\alpha+2}\Gamma(-\alpha-1,\beta\gamma)\\ &\quad+(\beta\gamma-2\beta\hat\omega_{\mathrm{T}}\hat M_{\mathrm{T}}-\alpha)\beta\gamma\mathrm{e}^{-\beta\gamma}\big\},\end{aligned} \tag{3.7}$$

where we have to substitute $\gamma = \gamma_{\min}^{\mathrm{T}}(\omega)$, cf. (3.5). The total transversal flux density is $F_\omega^{\mathrm{T}} = F_\omega^{\mathrm{T}(1)} + F_\omega^{\mathrm{T}(2)}$. The longitudinal density reads

$$\begin{aligned}\omega^k F_\omega^{\mathrm{L}} &= \frac{a_{\mathrm{t}}\mu(\omega)}{\Omega^2(\omega)}\frac{1}{(\beta\gamma)^{\alpha+2}}\frac{\varepsilon_0(\omega)\mu_0(\omega)}{\varepsilon(\omega)\mu(\omega)}\frac{\hat m_{\mathrm{t}}^2(\omega)}{M_{\mathrm{L}}^2}\frac{\omega^{1+k}}{\hat\omega_{\mathrm{L}}^2+1}\\ &\quad\times\big\{\big[\alpha(\alpha+1)+2(\alpha+1)\hat\omega_{\mathrm{L}}\beta\hat M_{\mathrm{L}}-\beta^2\hat M_{\mathrm{L}}^2\big]\\ &\quad\times(\beta\gamma)^{\alpha+2}\Gamma(-\alpha-1,\beta\gamma)\\ &\quad+(\beta\gamma-2\hat\omega_{\mathrm{L}}\beta\hat M_{\mathrm{L}}-\alpha)\beta\gamma\mathrm{e}^{-\beta\gamma}\big\},\end{aligned} \tag{3.8}$$

where we substitute $\gamma = \gamma_{\min}^{\mathrm{L}}(\omega)$ in (3.5). For a thermal electron distribution with $\alpha = -2$, the spectral functions simplify since $\Gamma(1,\beta\gamma) = \mathrm{e}^{-\beta\gamma}$. The unpolarized flux is $F_\omega^{\mathrm{T+L}} = F_\omega^{\mathrm{T}} + F_\omega^{\mathrm{L}}$.

In the semiclassical regime $\hat M_{\mathrm{T,L}} \ll 1$, cf. (3.4), it is convenient to factorize $\beta\gamma_{\min}^{\mathrm{T,L}}(\omega) = x_{\mathrm{T,L}}\eta_{\mathrm{T,L}}$, where, cf. (3.5),

$$x_{\mathrm{T,L}} = \beta\sqrt{1+\hat\omega_{\mathrm{T,L}}^2}, \qquad \eta_{\mathrm{T,L}} = \frac{\hat\omega_{\mathrm{T,L}}}{\sqrt{1+\hat\omega_{\mathrm{T,L}}^2}}\hat M_{\mathrm{T,L}} + \sqrt{1+\hat M_{\mathrm{T,L}}^2}. \tag{3.9}$$

We substitute $\beta\gamma = x_{\mathrm{T,L}}\eta_{\mathrm{T,L}}$ into the averaged spectral densities (3.6)–(3.8) and note that $\eta_{\mathrm{T,L}} \ge 1$ and $\eta_{\mathrm{T,L}}$ is also bounded from above for $\hat M_{\mathrm{T,L}} \ll 1$ and arbitrary $\hat\omega_{\mathrm{T,L}}$. We will use $x_{\mathrm{T,L}}$ as expansion parameter, which can be large or small depending on $0 < \beta < \infty$ and $\hat\omega_{\mathrm{T,L}}$.

4. Coinciding transversal and longitudinal dispersion relations in the quasiclassical regime

Identical dispersion relations require the identity $\varepsilon\mu = \varepsilon_0\mu_0$, cf. after (2.10). We can then drop the T and L subscripts of $M_{\mathrm{T,L}}$, $\hat M_{\mathrm{T,L}}$ and $\hat\omega_{\mathrm{T,L}}$, cf. (2.8) and (3.4), and also in (3.5) and (3.9), writing $\beta\gamma_{\min}(\omega) = x\eta$ and replacing $\beta\gamma$ by $x\eta$ in the spectral densities (3.6)–(3.8).

We scale the magnetic permeability μ into the fine-structure constant $\alpha_{\mathrm{t}}(\omega)$, cf. after (2.6),

$$\hat\alpha_{\mathrm{t}}(\omega) = \alpha_{\mathrm{t}}(\omega)\mu(\omega) = \frac{q^2}{4\pi}\frac{\mu(\omega)}{\Omega^2(\omega)}, \tag{4.1}$$

and specify the frequency dependence of $\hat\alpha_{\mathrm{t}}(\omega)$ and the rescaled tachyon mass $\hat m_{\mathrm{t}}(\omega)$ in (2.7) as power laws [32,33],

$$\hat\alpha_{\mathrm{t}}(\omega) = \hat\alpha_{\mathrm{t}0}\omega^\sigma, \qquad \hat m_{\mathrm{t}}(\omega) = \hat m_{\mathrm{t}0}\omega^\rho, \tag{4.2}$$

where $\hat\alpha_{\mathrm{t}0}$ and $\hat m_{\mathrm{t}0}$ are constant positive amplitudes, and σ and ρ are real exponents to be determined from spectral fits. Substituting $\hat m_{\mathrm{t}}(\omega)$ into the wave numbers (2.10), we find the tachyonic group velocity $\upsilon_{\mathrm{gr}} = 1/k'_{\mathrm{T,L}}(\omega)$ as

$$\upsilon_{\mathrm{gr}} - 1 \sim \left(\frac12 - \rho\right)\big(\omega^{\rho-1}\hat m_{\mathrm{t}0}\big)^2 + \mathrm{O}\big(\big(\omega^{\rho-1}\hat m_{\mathrm{t}0}\big)^4\big), \tag{4.3}$$

so that $v_{\rm gr}$ is superluminal for tachyonic mass exponents $\rho < 1/2$. It is also evident from (2.7) and (4.1) that the frequency dependence of the tachyon mass as well as the frequency-dependent factor Ω^2 of the tachyonic fine-structure constant can be absorbed into the permeabilities. That is, we can use a constant tachyon mass and fine-structure constant, employing dispersive permeabilities [9,34–36].

The amplitude factor $a_{\rm t}\mu/\Omega^2$ in flux densities (3.6)–(3.8) reads, cf. (3.4), (4.1) and (4.2),

$$\frac{a_{\rm t}\mu(\omega)}{\Omega^2(\omega)} = \hat{a}_{\rm t}\omega^\sigma, \quad \hat{a}_{\rm t} := \frac{\hat{\alpha}_{\rm t0}A_{\alpha,\beta}}{4\pi d^2}\beta^{\alpha-1}. \tag{4.4}$$

We further specialize the permeabilities as $\varepsilon\mu = \varepsilon_0\mu_0 = 1$, so that the variables in (2.8) and (3.4) simplify,

$$M = \hat{m}_{\rm t0}\omega^\rho, \qquad \hat{M} = \frac{\hat{m}_{\rm t0}}{2m}\omega^\rho, \qquad \hat{\omega} = \frac{\omega^{1-\rho}}{\hat{m}_{\rm t0}}. \tag{4.5}$$

The unpolarized flux is obtained by adding the averaged spectral densities (3.6)–(3.8),

$$\begin{aligned}\omega^k F^{\rm T+L}_\omega = \frac{\hat{a}_{\rm t}}{(x\eta)^{\alpha+2}}\frac{\omega^{\sigma+1+k}}{\hat{\omega}^2+1}2\Bigg\{\Bigg[\alpha(\alpha+1) + \frac{2(\alpha+1)\hat{\omega}}{\sqrt{1+\hat{\omega}^2}}\hat{M}x \\ - x^2\left(\frac{1}{2} - \hat{M}^2 + \frac{\hat{M}^2}{1+\hat{\omega}^2}\right)\Bigg](x\eta)^{\alpha+2}\Gamma(-\alpha-1, x\eta) \\ + \left(x\left(\eta - \frac{2\hat{\omega}}{\sqrt{1+\hat{\omega}^2}}\hat{M}\right) - \alpha\right)x\eta{\rm e}^{-x\eta}\Bigg\},\end{aligned} \tag{4.6}$$

where we substitute the variables, cf. (3.9) and (4.5),

$$x = \hat{\beta}\omega^{1-\rho}\sqrt{1+\frac{1}{\hat{\omega}^2}}, \quad \hat{\beta} := \frac{\beta}{\hat{m}_{\rm t0}}, \tag{4.7}$$

$$\eta = \frac{\hat{\omega}}{\sqrt{1+\hat{\omega}^2}}\hat{M} + \sqrt{1+\hat{M}^2}. \tag{4.8}$$

The independent fitting parameters are $\hat{a}_{\rm t}$, $\hat{\beta}$, $\hat{m}_{\rm t0}$, σ and ρ. We also note $\eta \to 1$ for $\hat{M} \to 0$. In a finite frequency interval defined by the available data sets, the semiclassical regime $\hat{M} \ll 1$ is realized for sufficiently small tachyon–electron mass ratio $\hat{m}_{\rm t0}/m$, cf. (4.5). If $\hat{\omega} \gg 1$ holds in addition to $\hat{M} \ll 1$ (which means $x \sim \hat{\beta}\omega^{1-\rho}$, cf. (4.5) and (4.7)), then $\hat{m}_{\rm t0}$ is not any more a fitting parameter, as it drops out of the flux density (4.6). We introduce the parameters

$$\begin{aligned}&A_\infty = \frac{\hat{a}_{\rm t}\beta^2}{\hat{\beta}^{\alpha+4}}, \qquad \eta_\infty = \eta_0 + (\alpha+2)(\rho-1), \\ &\eta_0 = \sigma + 2\rho - 1 + k,\end{aligned} \tag{4.9}$$

and replace the first two ratios in the flux density (4.6) by an identical expression,

$$\frac{\hat{a}_{\rm t}}{(x\eta)^{\alpha+2}}\frac{\omega^{\sigma+1+k}}{\hat{\omega}^2+1} \to \frac{A_\infty\omega^{\eta_\infty}}{(1+1/\hat{\omega}^2)^{\alpha/2+2}\eta^{\alpha+2}}, \tag{4.10}$$

so that we can use A_∞ and η_∞ in (4.9) as fitting parameters instead of $\hat{a}_{\rm t}$ and σ. Finally, in the case of a thermal source plasma with electron index $\alpha = -2$, the unpolarized flux (4.6) simplifies to

$$\begin{aligned}\omega^k F^{\rm T+L}_\omega = \frac{A_\infty\omega^{\eta_\infty}}{1+1/\hat{\omega}^2}{\rm e}^{-x\eta}2\Bigg\{2 - \frac{2\hat{\omega}}{\sqrt{1+\hat{\omega}^2}}\hat{M}x \\ - x^2\left(\frac{1}{2} - \hat{M}^2 + \frac{\hat{M}^2}{1+\hat{\omega}^2}\right) \\ + \left(x\left(\eta - \frac{2\hat{\omega}}{\sqrt{1+\hat{\omega}^2}}\hat{M}\right) + 2\right)x\eta\Bigg\},\end{aligned} \tag{4.11}$$

with $A_\infty = \hat{a}_{\rm t}\beta^2/\hat{\beta}^2$ and $\eta_\infty = \eta_0$, cf. (4.9).

5. Tachyonic Cherenkov fits to γ-ray pulsars in the GeV band

The quasiclassical regime is realized if the tachyon mass is small, $\hat{m}_{\rm t0}/m \ll 1$, and the electron gas ultra-relativistic, $\beta \ll 1$, so that the rescaled temperature variable $\hat{\beta}$ in (4.7) stays moderate. We can then approximate $x \sim \hat{\beta}\omega^{1-\rho}$, cf. (4.7), $\eta \sim 1$, cf. (4.8), and $\hat{M} \to 0$, $\hat{\omega} \to \infty$, cf. (4.5). Performing these approximations in the total flux density, we obtain, cf. (4.6) and (4.10),

$$\begin{aligned}\omega^k F^{\rm T+L}_{\omega,{\rm cl}} = A_\infty\omega^{\eta_\infty}\big\{\big[2\alpha(\alpha+1) - \big(\hat{\beta}\omega^{1-\rho}\big)^2\big] \\ \times \big(\hat{\beta}\omega^{1-\rho}\big)^{\alpha+2}\Gamma\big(-\alpha-1, \hat{\beta}\omega^{1-\rho}\big) \\ + 2\big(\hat{\beta}\omega^{1-\rho} - \alpha\big)\hat{\beta}\omega^{1-\rho}\exp\big(-\hat{\beta}\omega^{1-\rho}\big)\big\}.\end{aligned} \tag{5.1}$$

The transversal polarization component $F^{\rm T(1)}_\omega$ in (3.6) vanishes in this limit, so that the transversal radiation is linearly polarized; $\omega^k F^{\rm T(2)}_{\omega,{\rm cl}}$ is given by (5.1) with the two factors of 2 dropped, and $F^{\rm L}_{\omega,{\rm cl}} = F^{\rm T+L}_{\omega,{\rm cl}} - F^{\rm T(2)}_{\omega,{\rm cl}}$, cf. (3.8). For a thermal source plasma with electron index $\alpha = -2$,

$$\omega^k F^{\rm T+L}_{\omega,{\rm cl}} = A_\infty\omega^{\eta_\infty}\exp\big(-\hat{\beta}\omega^{1-\rho}\big)\big(4 + 4\hat{\beta}\omega^{1-\rho} + \big(\hat{\beta}\omega^{1-\rho}\big)^2\big). \tag{5.2}$$

The high-frequency limit $\hat{\beta}\omega^{1-\rho} \gg 1$ of flux density (5.1) reads

$$\begin{aligned}\omega^k F^{\rm T+L}_{\omega,{\rm cl}} \sim A_\infty\omega^{\eta_\infty}\exp\big(-\hat{\beta}\omega^{1-\rho}\big)\big(\hat{\beta}\omega^{1-\rho}\big)^2 \\ \times\left(1 + \frac{2-\alpha}{\hat{\beta}\omega^{1-\rho}} + \frac{\alpha^2-3\alpha-6}{(\hat{\beta}\omega^{1-\rho})^2} + \cdots\right).\end{aligned} \tag{5.3}$$

The attenuation factor $\exp(-\hat{\beta}\omega^{1-\rho})$ with tachyonic mass exponent $0 < \rho < 1$ causes the subexponential decay of the spectral tails determined by the Weibull slope $\delta = 1-\rho$. The leading order in (5.3) is entirely due to the longitudinally polarized flux component; the transversal radiation contributes the ratio $2/(\hat{\beta}\omega^{1-\rho})$ to the next-to-leading order.

The low-frequency limit $\hat{\beta}\omega^{1-\rho} \ll 1$ of the unpolarized flux (5.1) is

$$\begin{aligned}\omega^k F^{\rm T+L}_{\omega,{\rm cl}} = A_\infty\omega^{\eta_\infty}\Big\{\big(\hat{\beta}\omega^{1-\rho}\big)^{\alpha+2}\big[2\Gamma(1-\alpha) \\ - \big(\hat{\beta}\omega^{1-\rho}\big)^2\Gamma(-\alpha-1)\big] \\ + \big(\hat{\beta}\omega^{1-\rho}\big)^3\frac{\alpha+3}{\alpha^2-1} + {\rm O}\big(\big(\hat{\beta}\omega^{1-\rho}\big)^4\big)\Big\},\end{aligned} \tag{5.4}$$

which remains valid for integer $\alpha \geq -1$ if epsilon expansion is applied [12,37]. For electron indices $\alpha < 1$, the leading order of (5.4) reads

$$\omega^k F^{\rm T+L}_{\omega,{\rm cl}} \sim A_0\omega^{\eta_0}, \quad A_0 = \frac{\hat{a}_{\rm t}\beta^2}{\hat{\beta}^2}2\Gamma(1-\alpha), \tag{5.5}$$

with scaling exponent $\eta_0 = \sigma + 2\rho - 1 + k$, cf. (4.9). The amplitude ratio of the low- and high-frequency limits is $A_0/A_\infty = \hat{\beta}^{\alpha+2}2\Gamma(1-\alpha)$, cf. (4.9). In the low-frequency regime, the transversal and longitudinal flux components have equal strength, each contributing $A_0\omega^{\eta_0}/2$ to the flux (5.5).

In this section, we have studied the limit $\hat{M} \ll 1$, $\hat{\omega} \gg 1$, cf. (4.5). In particular, the low-frequency limit $\hat{\beta}\omega^{1-\rho} \ll 1$ in (5.4) and (5.5) was derived under the condition $\hat{\omega} \gg 1$. This is the relevant limit for γ-ray spectra. In the radio band, a different realization of the low-frequency limit of flux density (4.6) applies, namely $\hat{M} \ll 1$ and $\hat{\omega} \ll 1$, see Ref. [8]. In this case, we can approximate $x \sim \beta$, cf. (4.7), and $\eta \sim 1$, cf. (4.8), to find the low-frequency limit of density (4.6) as $\omega^k F^{\rm T+L}_{\omega,{\rm cl}} \sim \tilde{A}_0\omega^{\sigma+1+k}$, with amplitude

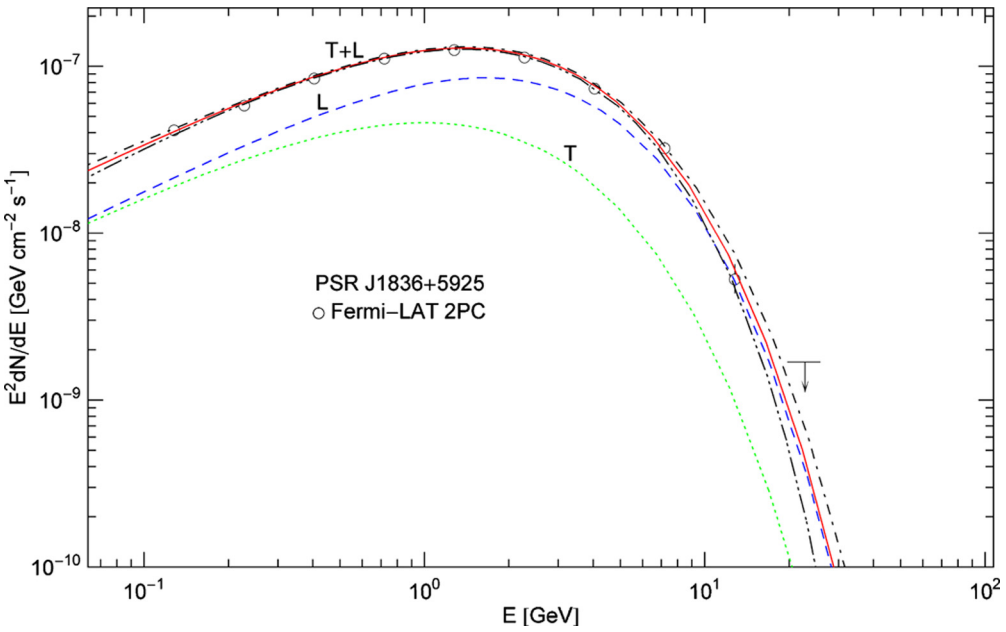

Fig. 1. Tachyonic γ-ray spectrum of pulsar PSR J1836+5925. Data points from Fermi-LAT (2nd Pulsar Catalog) [10,26]. The solid curve T + L depicts the unpolarized tachyonic energy flux $EF_E^{\mathrm{T+L}} = E^2\mathrm{d}N^{\mathrm{T+L}}/\mathrm{d}E$, cf. (3.3) and (5.2), obtained by adding the transversal flux component EF_E^{T} (dotted curve, labeled T) and the longitudinal component EF_E^{L} (dashed curve, L). The polarization components $EF_E^{\mathrm{T,L}}$ are compiled in (3.6)–(3.8). The dot-dashed and double-dot-dashed curves depict the upper and lower 2σ (95%) confidence limits of the χ^2 fit. The power-law ascent (5.5) is followed by a cross-over into subexponential Weibull decay, cf. (5.3). The spectral parameters listed in Table 1 are similar to Geminga [9]. The mass scaling exponent ρ lies below 1/2, which causes a rapid spectral cutoff and renders the radiation superluminal, cf. (4.3). The distance estimate for this pulsar is $d \approx 0.5 \pm 0.3$ kpc. (5 dof, $\chi^2 \approx 6.8$.)

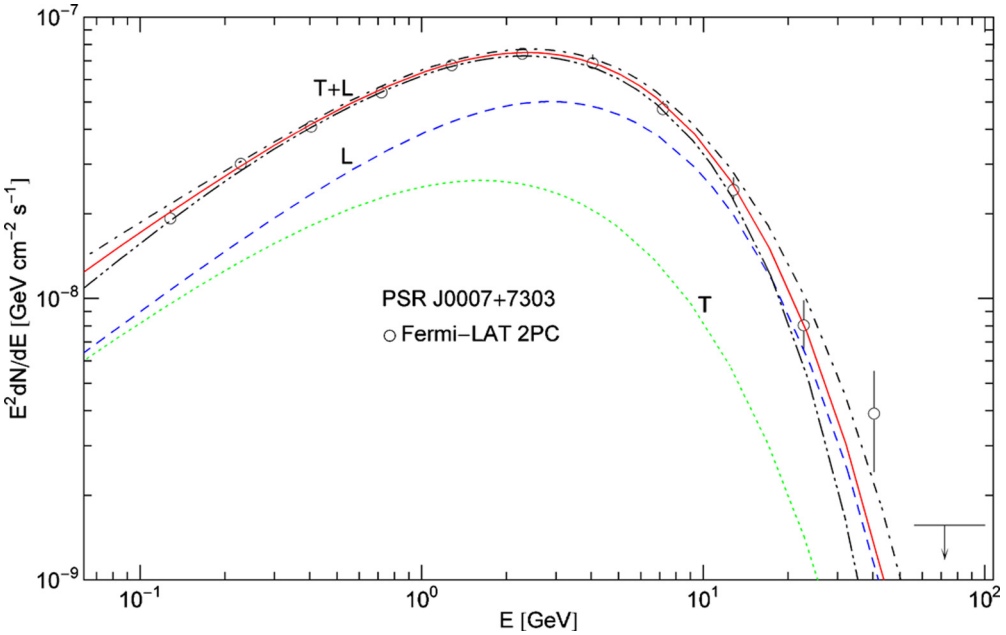

Fig. 2. Tachyonic energy flux of pulsar PSR J0007+7303. Data points from Fermi-LAT [10,27]. The caption to Fig. 1 applies. The polarization components are labeled T and L, the $\pm 2\sigma$ error band is indicated by the dot-dashed curves. The transversal radiation is linearly polarized and weaker than the longitudinal component. The scaling exponent ρ of the tachyon mass is about 1/2, cf. Table 1, which is just the border between sub- and superluminality, cf. (4.3). $d \approx 1.4 \pm 0.3$ kpc. (7 dof, $\chi^2 \approx 6.2$.)

$$\tilde{A}_0 = \frac{\hat{a}_{\mathrm{t}}}{\beta^{\alpha+2}}\big[\big(2\alpha(\alpha+1)-\beta^2\big)\beta^{\alpha+2}\Gamma(-\alpha-1,\beta) + 2(\beta-\alpha)\beta \mathrm{e}^{-\beta}\big]. \tag{5.6}$$

This replaces the flux limit (5.5) in a frequency regime where $\hat{\omega} \ll 1$. In the GeV γ-ray band, we employ flux density (5.1) and its high- and low-frequency limits (5.3) and (5.5).

In the spectral fits of the γ-ray pulsars depicted in Figs. 1–4, we use a thermal electron index $\alpha = -2$. First, we perform a low-frequency power-law fit (5.5) to estimate A_0 and η_0. In this way, we also find initial estimates of A_∞ and η_∞, see (4.9) and after (5.5). Estimates of $\hat{\beta}$ and ρ are then obtained by fitting the spectral tail (5.3). Finally, using these estimates as initial guess for the fitting parameters A_∞, η_∞, $\hat{\beta}$ and ρ, we perform a least-squares χ^2 fit with flux density (5.2), cf. Table 1.

6. Conclusion: spectral decay and the extreme quantum regime

The basic results have been summarized in the introduction. Here, we conclude with some remarks on Weibull decay of spectral

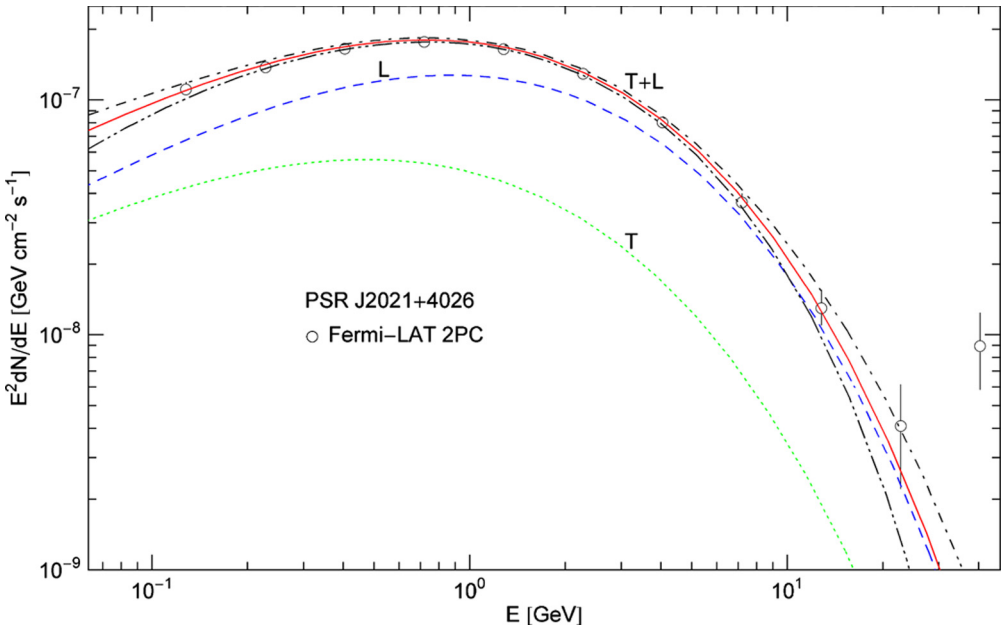

Fig. 3. Tachyonic γ-ray spectrum of pulsar PSR J2021+4026. Data points from Fermi-LAT [10,28], the caption to Fig. 1 applies. The tachyonic mass scaling exponent ρ lies above 1/2, resulting in a gradual spectral cutoff and in subluminal γ-rays, cf. (4.3). The spectral parameters in Table 1 are similar to the Vela pulsar [9]; the spectral peak is located at about the same energy, as the larger decay exponent $\hat{\beta}$ is compensated by the smaller shape parameter $1-\rho$, cf. (5.3). (The flux amplitude a_t of the pulsars discussed in [9] corresponds to $A_\infty\hat{\beta}^2$, cf. Table 1, and the decay exponent β_∞ in [9] to $\hat{\beta}$.) The pulsar distance is $d \approx 1.5 \pm 0.4$ kpc. (6 dof, $\chi^2 \approx 1.3$.)

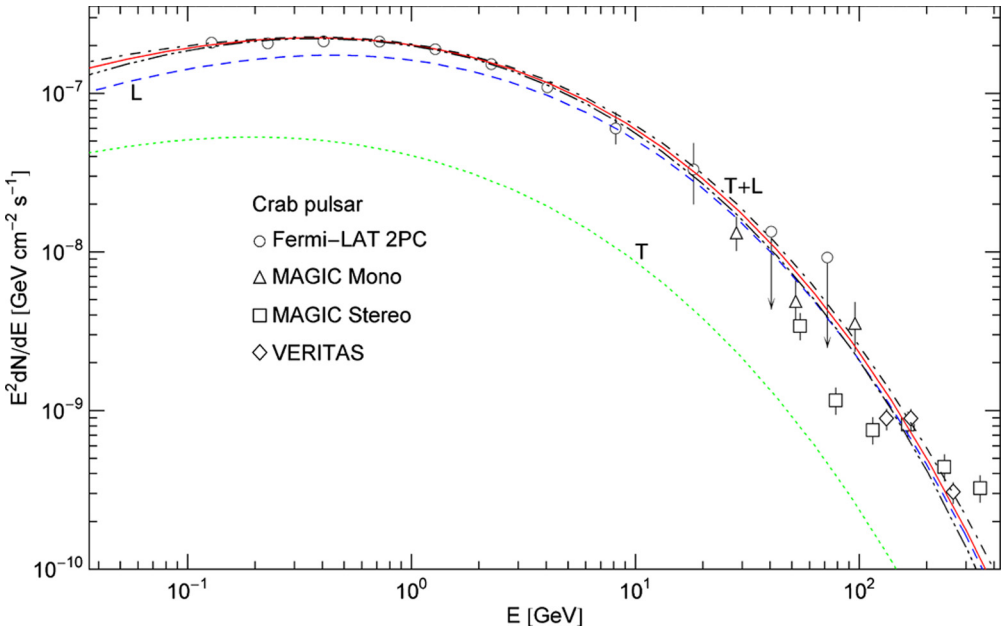

Fig. 4. Tachyonic energy flux of the Crab pulsar PSR J0534+2200. Data points from Fermi-LAT [10,29], MAGIC [11,30] and VERITAS [31]. The caption to Fig. 1 applies. The emission is subluminal, the Weibull shape parameter of the spectral tail is noticeably smaller ($1-\rho \approx 0.2$) and the decay exponent $\hat{\beta}$ larger than of the other pulsars, cf. Table 1. A Weibull exponential with small shape parameter and large decay exponent can approximate power-law decay over a finite energy range, cf. (5.3) and (6.2), although the spectral tail remains slightly curved and thus distinguishable from a power-law slope (linear in a double-logarithmic plot). $d \approx 2.0 \pm 0.5$ kpc. (14 dof, $\chi^2 \approx 67$.)

Table 1
Parameters of the tachyonic energy flux of the pulsars in Figs. 1–4. The γ-rays are radiated by a thermal plasma with electron index $\alpha = -2$, cf. (3.1). The fine-structure scaling exponent $\sigma = \eta_\infty - 2\rho$ is inferred from the scaling exponent ρ of the tachyon mass, cf. (4.2), and from the exponent η_∞ in (4.9) determining the slope of the initial power-law ascent of the flux density. The fitting parameters are η_∞, ρ, the decay exponent $\hat{\beta}$, cf. (4.7), and the flux amplitude A_∞, cf. (4.9). The spectral fits depicted in the figures are based on the differential flux density $EF_E^{T+L} = E^2 dN^{T+L}/dE$, cf. (3.3) and (5.2). The Weibull shape parameter determining the subexponential decay of the spectral tails is $1-\rho$, cf. (5.3). The indicated standard deviations are extracted from the covariance matrix of the χ^2 functional.

	σ	ρ	η_∞	$\hat{\beta}$ [GeV^{-1}]	A_∞ [GeV cm^{-2} s^{-1}]
PSR J1836+5925	-0.013	0.419 ± 0.029	0.826 ± 0.045	2.10 ± 0.19	$6.04 \pm 0.60 \times 10^{-8}$
PSR J0007+7303	-0.259	0.504 ± 0.042	0.749 ± 0.062	1.73 ± 0.29	$2.57 \pm 0.36 \times 10^{-8}$
PSR J2021+4026	-0.436	0.630 ± 0.051	0.824 ± 0.183	3.93 ± 0.10	$2.55 \pm 1.69 \times 10^{-7}$
Crab pulsar	-0.824	0.809 ± 0.019	0.795 ± 0.159	6.83 ± 1.45	$2.40^{+2.70}_{-2.40} \times 10^{-6}$

tails, polarization and the quantum limit. We have not discussed the extreme quantum limit of the flux densities (3.6)–(3.8) (realized by large tachyon–electron mass ratios $\hat{M}_{\mathrm{T,L}}(\omega)\gg 1$, cf. (3.4)) in any detail, as the spectral fits in Figs. 1–4 are performed in the quasiclassical regime.

6.1. Sub- and superexponential decay of spectral tails

The second-quantized flux densities (3.6)–(3.8) decay for large electronic Lorentz factors, since $(\beta\gamma)^{\alpha+2}\Gamma(-\alpha-1,\beta\gamma)\sim \mathrm{e}^{-\beta\gamma}$. The minimal transversal/longitudinal Lorentz factor $\gamma^{\mathrm{T,L}}_{\mathrm{min}}(\omega)$ in (2.14) increases at least linearly with ω, so that the ultimate decay of the flux densities is exponential or superexponential for $\omega\to\infty$. In contrast, if ω varies in a finite interval (defined by data sets) and the tachyonic mass amplitude $\hat{m}_{\mathrm{t}0}$ is sufficiently small and the electron temperature high, then the approximation $\beta\gamma^{\mathrm{T,L}}_{\mathrm{min}}\sim\hat{\beta}\omega^{1-\rho}$ used in (5.1) and (5.2) is applicable in this interval, and the decay factor $\exp(-\hat{\beta}\omega^{1-\rho})$ in the flux density (5.3) is subexponential for $0<\rho<1$ and superexponential for negative ρ. Subexponential decay within a finite interval can be realized in the quasiclassical regime, where the mass ratios $\hat{M}_{\mathrm{T,L}}$ defined in (2.8) and (3.4) are small, but also in the opposite limit, the extreme quantum regime where $\hat{M}_{\mathrm{T,L}}(\omega)\gg 1$, see the following remark.

6.2. Spectral decay and polarization in the quantum limit

Instead of using the factorization (3.9) designed for the quasiclassical regime, we split the minimal Lorentz factor as $\beta\gamma^{\mathrm{T,L}}_{\mathrm{min}}(\omega)=y_{\mathrm{T,L}}\kappa_{\mathrm{T,L}}$, where, cf. (3.5),

$$y_{\mathrm{T,L}}=\beta\hat{M}_{\mathrm{T,L}}\sqrt{1+\hat{\omega}^2_{\mathrm{T,L}}},\qquad \kappa_{\mathrm{T,L}}=\frac{\hat{\omega}_{\mathrm{T,L}}}{\sqrt{1+\hat{\omega}^2_{\mathrm{T,L}}}}+\sqrt{1+\frac{1}{\hat{M}^2_{\mathrm{T,L}}}},\tag{6.1}$$

and substitute $\beta\gamma=y_{\mathrm{T,L}}\kappa_{\mathrm{T,L}}$ into the flux densities (3.6)–(3.8). The factor $\kappa_{\mathrm{T,L}}$ is larger than one and also bounded from above for $\hat{M}_{\mathrm{T,L}}(\omega)\gg 1$ (quantum regime) and arbitrary $\hat{\omega}_{\mathrm{T,L}}$, cf. (4.5). The expansion parameter in the flux densities is now $y_{\mathrm{T,L}}$, which can be large or small, depending on β, $\hat{\omega}_{\mathrm{T,L}}$ and $\hat{M}_{\mathrm{T,L}}\gg 1$. As in Section 4, we assume permeabilities constrained by $\varepsilon\mu=\varepsilon_0\mu_0=1$, which give identical mass-squares $M^2_{\mathrm{T,L}}$ for transversal and longitudinal quanta, cf. (2.8), and specify the frequency scaling of the tachyon mass and the tachyonic fine-structure constant as stated in (4.2). We can then drop the T and L subscripts in (6.1) and consider a finite frequency interval in which $\hat{\omega}\ll 1$ holds, cf. (4.5), so that $\beta\gamma=y\kappa\sim\beta\hat{M}=\hat{\beta}_{\mathrm{q}}\omega^{\rho}$ with $\hat{\beta}_{\mathrm{q}}=\beta\hat{m}_{\mathrm{t}0}/(2m)$, uniformly within this interval. For $y\kappa\gg 1$, the decay factor $\exp(-y\kappa)$ of the spectral tails is thus subexponential if $0<\rho<1$ and superexponential for $\rho>1$. (The quasiclassical counterpart is the Weibull exponential in (5.3), albeit in the opposite limit $\hat{\omega}\gg 1$, $\hat{M}\ll 1$.) For $\hat{\omega}\gg 1$ and $\hat{M}\gg 1$, we find strictly exponential decay with linear $y\kappa\sim\beta\omega/m$, cf. (4.5) and (6.1). The polarization changes in the quantum regime; there are two transversal degrees, cf. (3.6) and (3.7), which are of comparable magnitude for $y\kappa\gg 1$, whereas the longitudinal flux (3.8) is weaker by a factor $1/(y\kappa)$. Polarization in the quasiclassical regime has been discussed in Section 5.

6.3. Subexponential decay approximating power-law decay in the quasiclassical regime

If the scaling exponent ρ of the tachyon mass in (4.2) is close to one, $0<1-\rho=\varepsilon\ll 1$, then the Weibull exponential $\exp(-\hat{\beta}\omega^{1-\rho})$ in the flux asymptotics (5.3) admits the epsilon expansion

$$\exp\bigl(-\hat{\beta}\omega^{\varepsilon}\bigr)\sim \mathrm{e}^{-\hat{\beta}}\omega^{-\hat{\beta}\varepsilon}\left(1-\frac{1}{2}\hat{\beta}\varepsilon^2\log^2\omega+\mathrm{O}\bigl(\hat{\beta}\varepsilon^3,\hat{\beta}^2\varepsilon^4\bigr)\right).\tag{6.2}$$

If the decay exponent $\hat{\beta}$ is large, so that $\hat{\beta}\varepsilon$ is moderate, this expansion approximates power-law decay $\propto\omega^{-\hat{\beta}\varepsilon}$, leading to slightly curved spectral tails in double-logarithmic plots, see the spectral fit of the Crab pulsar in Fig. 4 and Table 1. Alternatively, one may consider a logarithmic frequency dependence of the tachyon mass from the outset, replacing the power law $\hat{m}_{\mathrm{t}}(\omega)=\hat{m}_{\mathrm{t}0}\omega^{\rho}$ in (4.2) by $\hat{m}_{\mathrm{t}}(\omega)=\hat{m}_{\mathrm{t}0}\omega/\log(1+\hat{m}_{\mathrm{t}1}\omega^{\rho})$. The semiclassical expansion parameter $x\sim\hat{\beta}\omega^{1-\rho}$ in the flux densities is then replaced by $\hat{\beta}\log(1+\hat{m}_{\mathrm{t}1}\omega^{\rho})$, cf. the beginning of Section 5, so that the Weibull exponential in (5.3) becomes a power law $(1+\hat{m}_{\mathrm{t}1}\omega^{\rho})^{-\hat{\beta}}$. In contrast, the spectral fits of the pulsars in Figs. 1–4 are based on the tachyonic mass scaling relation (4.2), resulting in subexponential Weibull decay of the GeV spectral tails because of the attenuation factor $\exp(-\hat{\beta}\omega^{1-\rho})$ in the high-frequency asymptotics (5.3) of the Cherenkov flux.

References

[1] P.A. Caraveo, Annu. Rev. Astron. Astrophys. 52 (2014), arXiv:1312.2913.
[2] W. Weibull, J. Appl. Mech. 18 (1951) 293.
[3] V.L. Ginzburg, V.N. Tsytovich, Transition Radiation and Transition Scattering, Hilger, Bristol, 1990.
[4] V.L. Ginzburg, Phys. Usp. 39 (1996) 973.
[5] V.L. Ginzburg, Phys. Usp. 45 (2002) 341.
[6] G.N. Afanasiev, Vavilov–Cherenkov and Synchrotron Radiation, Kluwer, Dordrecht, 2004.
[7] G.N. Afanasiev, M.V. Lyubchenko, Yu.P. Stepanovsky, Proc. R. Soc. A, Math. Phys. Eng. Sci. 462 (2006) 689.
[8] R. Tomaschitz, Phys. Lett. A 377 (2013) 3247.
[9] R. Tomaschitz, Europhys. Lett. 106 (2014) 39001.
[10] A.A. Abdo, et al., Astrophys. J. Suppl. Ser. 208 (2013) 17.
[11] J. Aleksić, et al., Astron. Astrophys. 540 (2012) A69.
[12] R. Tomaschitz, Ann. Phys. 322 (2007) 677.
[13] R. Tomaschitz, Europhys. Lett. 102 (2013) 61002.
[14] Ya.P. Terletsky, Sov. Phys. Dokl. 5 (1961) 782.
[15] R.A. Treumann, Europhys. Lett. 16 (1991) 121.
[16] V.L. Ginzburg, Phys. Scr. T 2A (1982) 182.
[17] R. Tomaschitz, Eur. Phys. J. C 49 (2007) 815.
[18] R. Tomaschitz, Physica A 320 (2003) 329.
[19] R. Tomaschitz, J. Phys. A, Math. Gen. 38 (2005) 2201.
[20] R. Tomaschitz, Eur. Phys. J. D 32 (2005) 241.
[21] H. Chen, M. Chen, Mater. Today 14 (2011) 34.
[22] R. Tomaschitz, Physica A 387 (2008) 3480.
[23] R. Tomaschitz, Physica B 405 (2010) 1022.
[24] R. Tomaschitz, Europhys. Lett. 104 (2013) 19001.
[25] R. Tomaschitz, Physica A 394 (2014) 110.
[26] A.A. Abdo, et al., Astrophys. J. 712 (2010) 1209.
[27] A.A. Abdo, et al., Astrophys. J. 744 (2012) 146.
[28] A.A. Abdo, et al., Astrophys. J. 700 (2009) 1059.
[29] A.A. Abdo, et al., Astrophys. J. 708 (2010) 1254.
[30] J. Aleksić, et al., Astrophys. J. 742 (2011) 43.
[31] E. Aliu, et al., Science 334 (2011) 69.
[32] R. Tomaschitz, Eur. Phys. J. C 69 (2010) 241.
[33] R. Tomaschitz, Europhys. Lett. 89 (2010) 39002.
[34] R. Tomaschitz, Physica A 307 (2002) 375.
[35] R. Tomaschitz, Opt. Commun. 282 (2009) 1710.
[36] R. Tomaschitz, Phys. Lett. A 377 (2013) 945.
[37] R. Tomaschitz, Appl. Math. Comput. 225 (2013) 228.